Received: 10 January 2023 | Revised: 19 March 2023 | Accepted: 26 March 2023

DOI: 10.1002/eng2.12660

RESEARCH ARTICLE

Engineering Reports Open Access WILEY

A computational convection analysis of SiO_2/water and MoS_2-SiO_2/water based fluidic system in inverted cone

Syed Ibrar Hussain[1] | **Iftikhar Ahmad**[2] | **Muhammad Asif Zahoor Raja**[3] | **Ch Muhammad Zulfiqar Umer**[2]

[1]Dipartimento di Matematica e Informatica, Università degli Studi di Palermo, Via Archirafi 34, Palermo, 90123, Italy

[2]Department of Mathematics, University of Gujrat, Gujrat, 50700, Pakistan

[3]Future Technology Research Center, National Yunlin University of Science and Technology, 123 University Road Douliu, 64002, Yunlin, Taiwan

Correspondence
Syed Ibrar Hussain, Dipartimento di Matematica e Informatica, Università degli Studi di Palermo, Via Archirafi 34, 90123, Palermo, Italy.
Email: syedibrar.hussain@unipa.it

Abstract

A complete shape factor investigation of water-based mixture type hybrid nanofluid in a permeable boundary with the impact of magnetic field, thick dissemination, and warm radiation is presented in this article. A computational convection analysis of an inverted semi vertical cone with a porous surface in the form of SiO_2/water nanofluid and MoS_2-SiO_2/water hybrid nanofluid transport is developed. The system of differential equations is presented and solved numerically by the Lobatto IIIA method. The temperature distributions and fluid velocity are studied along with the coefficient of skin friction and the Nusselt number, taking into account the form of distinct nano-particles. The flow problem's results are approximated by using several embedding variables. Tables and graphs are constructed for a variety of scenarios including maximum residual error, mesh points, and Nusselt numbers. We conclude that boundary film thickness reduces and the fluid flow is resisted by magnetic field presence. Fluid flow slows down as λ increases, and this reduction is more evident in nanofluids than in hybrid nanofluids. With an increment in S, velocity drops. A detailed analysis of the proposed ordinary differential equations, boundary conditions, and numerical data of skin friction is given both in tabular and graphical forms. Additionally, it is observed that the fluid flow slows down more for the hybrid nanofluid than for the SiO_2/water nanofluid. Moreover, it is clear that the temperature increase for the SiO_2/water nanofluid is substantially greater. The authors deduce that the existence of a magnetic field resists fluid flow for hybrid nanofluid forms and decreases the thickness of the viscous boundary layer.

KEYWORDS

hybrid nanofluid (HNF), isothermal cone, Lobatto IIIA approach, nanofluid (NF), porous medium (PM), shape factors

1 | INTRODUCTION

The **base fluids** with low viscosity and thermal conductivity, such as glycol, water, and alcohol cannot be employed solely in many applications of science and technology because of their structure and limited properties. Due to this

vulnerability, a new class of fluid called NFs has been introduced. Such NFs are frequently utilized for macroscopic cooling because of the crucial characteristics of heat transport. The single-phase modeling approach of NFs is especially important for lubricant refining, coolants, and applications in daily life including portable computer systems, air conditioners, coolers, and nanostructures.[1] In the manufacturing industry, solar thermal collectors are recognized as a highly straightforward and environmentally friendly way to convert UV irradiation to heat energy.[2,3] In such collectors, various fluids such as glycol and water are used to improvise their performance and power.[4,5] Recently, numerically and experimentally, several researchers have researched the use of NFs in many kinds of solar collectors.[6,7] Many researchers and engineers have recently shown a strong interest in the subject of two-dimensional axially symmetric fluid motion inside a quasi-inverted cone. These flows offer important applications in a variety of engineering and manufacturing processes, such as the design of sustainable power plant equipment, gas turbines, propulsion systems for aircraft, spacecraft, missiles, satellites, storage of grains, the disposal of nuclear waste, the spread of chemical contaminants through water-saturated soil, and other processes that involve the movement of moisture through air trapped in fiber insulations.[8,9]

A **hybrid nanofluid** (HNF) covers nano-particles of various sorts. Synergistic results provide the HNF to integrate advantages from component nano-particles but avoid their drawbacks. This feature results in the properties of HNF as compared to mono-particle-based NFs.[10] Because of the minute size of the nano-particles and their very large common surface area, NFs have useful properties such as high-temperature conductivity, durable stability, minimum obstruction in flow passes, and homogeneity.[11,12] Choi and Eastman developed the idea of NFs for the suspension of ultrafine particulate liquids.[13] Khan and Pop have found the issue of flow over the stretch sheets in their initial work on NF.[14]

In this research, a complete shape factor investigation of water-based mixture NF in a permeable boundary alongside the impact of transverse attractive field, thick dissemination, and warm radiation is given. This article presents a computational convection analysis of an inverted cone with a porous surface in the form of SiO_2/water NF and MoS_2-SiO_2/water hybrid NF transport. Temperature distributions and NF velocity are studied, along with the coefficient of Nusselt number and the skin friction, taking into account the form of distinct nano-particles. The system of differential equations was simplified and numerically solved using the Lobatto IIIA method. The main findings from the present research are that the existence of a magnetic field resists flow for NF and HNF forms and decreases the thickness of the viscous boundary layer.

Ramzan described the modeling across a linear and significantly stretching layer of such a two-dimensional natural flow assessment of Williamson fluid.[15] NFs are arranged by dissolving the nano-particles in the base fluid and can considerably improve the heat conduction and get a heat transfer rate resembling that of pure fluids. NFs introduced by Choi have thermal conductivities in magnitudes, more than the conductivities of the base fluids, and with sizes suggestively smaller than 100 nm. The presence of nano-particles upgrades the warmth move execution of the base fluid fundamentally.

In 1979, Chiou calculated the laminar convection flow in the cone frustum. It was assumed that the temperature and the heat flux of the wall not changing and then reached a conclusion that the temperature was inversely proportional to the Prandtl number when moving along the wall of frustum.[16] Yih studied heat transfer and mass transfer of heat (convection) over an inverted cone with the porous medium have to change wall temperature and flux.[17]

EL-Aziz studied the numerical solution to investigate the effects of the time-dependent chemical reactions on the heat and mass transfer of NF and stagnation point flow on the stretching surface.[18] The authors of this research article have done some previous works in the field of differential equations, especially on non-linear partial differential equations by using a numerical technique to ensure the stability and convergence of the obtained results.[19-22] Recently, Ahmad et al. has worked on a HNF and NF models by using the Lobatto IIIA technique for obtaining the solution of fluidic models.[23]

A few years ago, Noghrehabadi discussed convection through NF over standing plates pasted in permeable medium surface heat flux in Reference 24. Water flow, glycol, and ethylene-based NF flow having natural convection through vertical cone on a PM are given in Reference 25. This research was extended by Ellahi, he found the effects of shape and size of nano-particles on entropy.[26] Namburu calculated copper oxide's viscosity in nano-particles suspended in ethylene glycol and H_2O mixtures. Later, he found a relationship between particle volume viscosity and temperature based on the data. They studied the rheological comportment of NFs.[27] It was observed by Chen that the shear thinning behavior of NFs was dependent on the thickness of particles, viscosity, and fluid flow rate.[28] Chan and Dinge studied the behavior of NFs having titanite as constituent nano-particles. They concluded that titanite has very strong thinning properties for

NFs and also, they have a huge impact on the concentration and temperature of the medium.[29] Then the results obtained were matched with other results of experiments on various kind of particles, and it showed a very good resemblance with their results.[30] Afshaari and Akbaree examined the nano-particles effects on the viscosity of NFs where it was determined that viscosity increases with the rise of volume fraction of nano-particles.[31] Kaang and Kime discussed natural convection which is a type of heat transfer in which fluids flow does not depend on an outer source. They also discussed some examples related to the research work.[32]

Lobatto IIIA method is applied for the numerical investigation of differential equations which are described by the use of approximations to the solution at endpoints. Due to strong stability properties, Lobatto IIIA methods have been considered for boundary value problems (BVP). We use the Lobatto IIIA method for numerical treatment since it is stiffly accurate. In this work, the authors have presented the analysis for the various values of mesh points and real tolerance to check the efficiency, stability, and reliability of proposed technique. In this research work, we analyzed the results of cross diffusion into a porous medium on the skin friction coefficient, mass and heat transfer from cone into a porous medium. A Lobatto IIIA method is used to find numerical solutions for energy, concentration, and momentum equations. A complete implementation strategy of the Lobatto IIIA method is demonstrated step by step in Figure 1 in a comprehensive manner. The Figure 1 expresses the graphical illustration of the proposed methodology by stating the problems, both NF and HNF, and its numerical computing procedure in an extensive manner. Using the Lobatto IIIA method, Nagoor[33] explained numerically the effect of different physical constraints on velocity and temperature fields for Darcy-Forchheimer HNF flow in revolving frames. The above-mentioned experiments in which many researchers presumed different fluids with various nano-particles and observed interesting findings for their thermophysical behavior are the motivation behind this proposed study. There is substantial research being conducted on the numerical approach to the problem of NF flow,[34-37] but relatively few researchers have attempted to solve the problem of hybrid flow of NF using special numerical methods. The present article offers a detailed form study of MoS_2-SiO_2/water water-dependent HNF inside a semi vertical and inverted cone having porous boundary as well as the impact of the presence of the magnetic field, viscous dissipation including thermal radiation.

The following are a few of the important aspects of this research:

- The radiative flow of HNFs MoS_2-SiO_2/water over a semi-inverted cone with porous boundary effects has been modeled in a novel way, using the power of sufficient similarity transformations, PDEs describing the flow model are converted into a system of ODEs.
- A computational investigation by exploiting the Lobatto IIIA approach is implemented for the dynamical analysis of a hybrid nanofluidic system passed over a semi-inverted cone with a porous boundary.
- The primary approach of boundary layer approximations is applied to systemize the governing nonlinear PDEs of the nanofluidic and hybrid nanofluidic model and these PDEs are converted into ODEs by the competence of similarity variables.
- The implementation of a numerical approach namely Lobatto IIIA technique that relates to the categories of finite difference numerical techniques for examining the nanofluidic model, is a novel work.
- The graphical illustration of each fluidic parameter on velocity and temperature fields is portrayed along with the numerical computed data of skin friction coefficient and Nusselt-number for assessment analysis.

The rest of the sections of the manuscript are cataloged as follows: Section 2 describes flow equation modeling, Section 3 provides numerical results and discussion and Section 4 summarizes the fluidic system's conclusion and recommendations.

2 | MODELING AND SIMULATION OF NANOFLUIDIC EQUATIONS

The development of physical problems involves an isothermic cone with an inverted porous medium in which the flow of an NF is a 2D steady-state and incompressible, is presented. ω is a semi-vertical angle along with the cone. The origin of the cartesian coordinates system is taken from vertex of cone.

Moreover, we chose the x-axis and y-axis as parallel and perpendicular to surface of inverted cone, respectively. The physical abstract of proposed model is illustrated in Figure 2. Considering the existence of viscous properties and

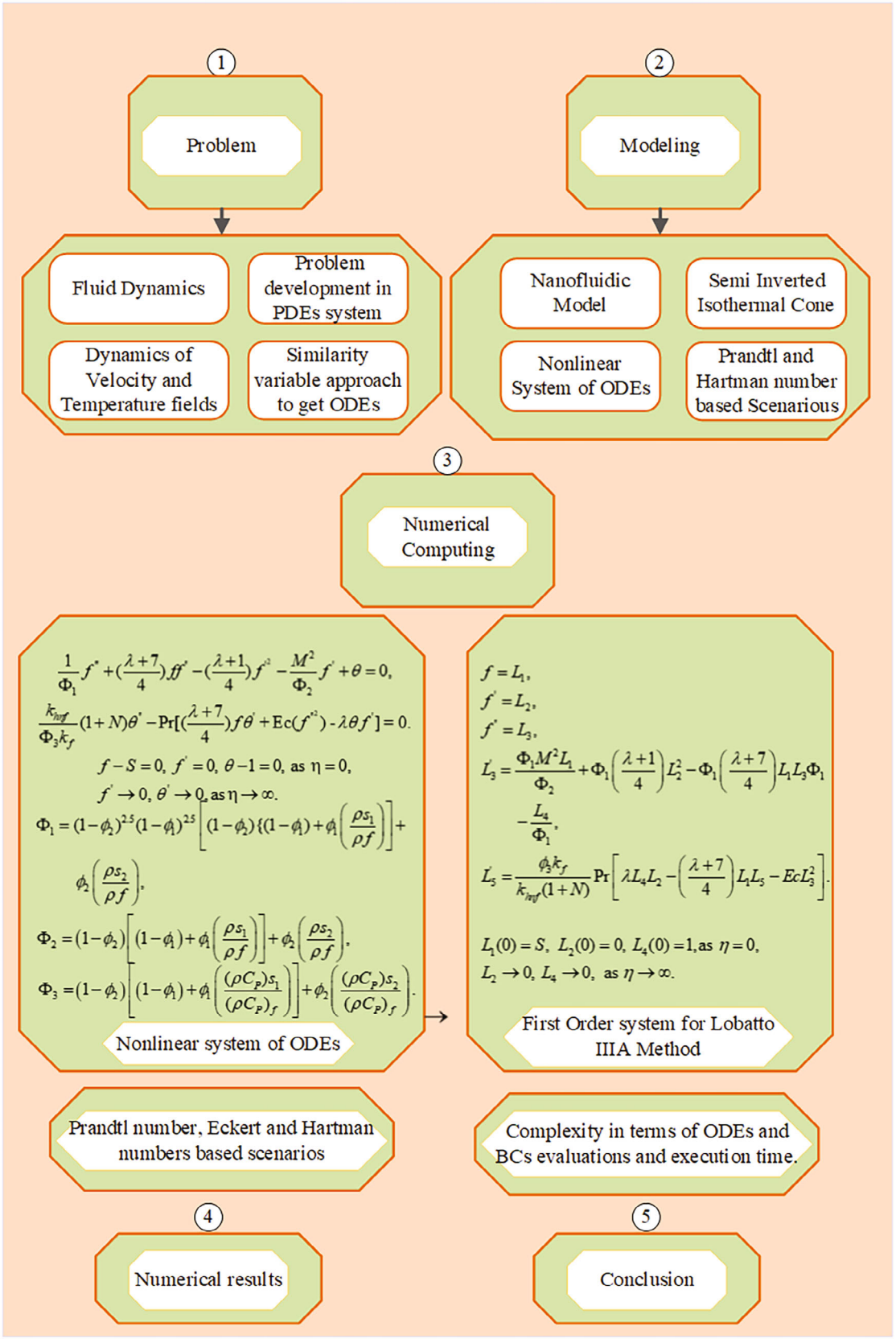

FIGURE 1 Graphical illustration of numerical methodology.

the effects of thermal energy, heat transmission is involved on surface of the cone (inverted). Figure 2 expresses the problem statement of the inverted cone model in x, y coordinate system. Table 1 presents the experimental values for different parameters of fluidic systems. Tables 2 and 3 represents the experimental values and properties of various parameters for the case of nanofluidic and hybrid nanofluidic systems, respectively. Also, we take temperature T as a constant value.[38] The temperature of the wall of an inverted cone is defined as $T_w = ax^{\lambda} + T_{\infty}$ where a($a > 0$) is constant and T_{∞} is temperature distant from the cone surface and its property is $T_{\infty} > T_{\infty}$. Also, λ is power index law. Under these assumptions, along with the approximations of boundary layers, the governing equations are determined as follow:

$$\frac{\partial}{\partial x}(ur) + \frac{\partial}{\partial y}(vr) = 0, \tag{1}$$

$$u\frac{\partial u}{\partial x} + v\frac{\partial u}{\partial y} = \frac{1}{\rho_{hnf}}\left[\mu_{hnf}\frac{\partial^2 u}{\partial y^2} + g(\rho\beta)_{hnf}(T - T_{\infty}) - \sigma^2\beta^2 u\right], \tag{2}$$

$$u\frac{\partial T}{\partial x} + v\frac{\partial T}{\partial y} = \frac{\mu_{hnf}}{(\rho c_p)_{hnf}}\left[\left(\frac{\partial u}{\partial y}\right)^2 - \frac{1}{\mu_{hnf}}\frac{\partial q_r}{\partial y}\right] + \alpha_{hnf}\frac{\partial^2 T}{\partial y^2}. \tag{3}$$

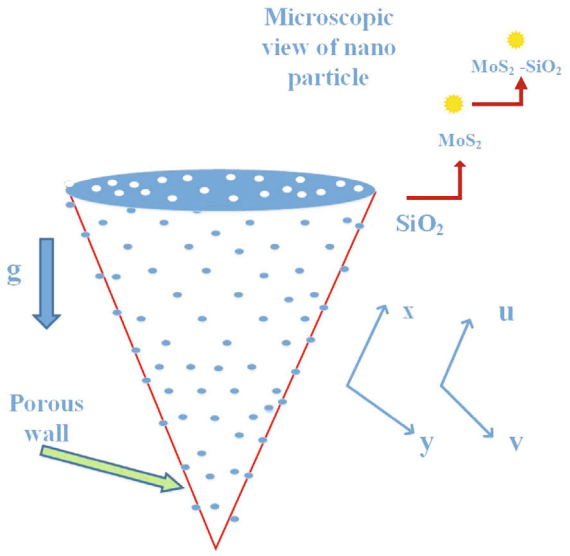

FIGURE 2 Illustration of physical problem in cartesian coord.

TABLE 1 Experimental values for fluidic system.

Properties	H_2O	SiO_2	MoS_2
Specific heat, C_p (J/kg K)	4179	730	397.746
Density, $\tilde{\rho}$ (kg/m^3)	0.613	1.5	34.5
Thermal conductivity, $\tilde{k}$ (W/mk)	997	2650	5060

TABLE 2 Experimental values for NF system.

Properties	NF
Viscosity	$\mu_{nf} = \frac{\mu_f}{(1-\varphi)^{2.5}}$
Density	$\rho_{nf} = \rho_f(1-\varphi) + \varphi(\rho_s)$
Thermal conductivity	$\frac{k_{nf}}{k_f} = \frac{k_s+(m-1)k_f-\varphi(m-1)(k_f-k_s)}{k_s+(m-1)k_f+(k_f-k_s)}$
Heat capacity	$(\rho c_p)_{nf} = (\rho c_p)_f(1-\varphi) + \varphi(\rho c_p)_s$

TABLE 3 Experimental values for HNF system.

Properties	Hybrid NF
Viscosity	$\mu_{hnf} = \frac{\mu_f}{(1-\varphi_1)^{2.5}(1-\varphi_2)^{2.5}}$
Density	$\rho_{hnf} = \rho_f(1-\varphi_2)\left[(1-\varphi_1)+\varphi_1\left(\frac{\rho_{s_1}}{\rho_f}\right)\right]+\varphi_2\rho_{s_2}$
Thermal cond.	$\frac{k_{hnf}}{k_f} = \frac{k_{s_2}+(m-1)k_{bf}-\varphi_2(m-1)\left(k_{bf}-k_{s_2}\right)}{k_{s_2}+(m-1)k_{bf}+\left(k_{bf}-k_{s_2}\right)}$
Heat Cap.	$(\rho c_p)_{hnf} = (\rho c_p)_f(1-\varphi_2)\left[(1-\varphi_1)+\varphi_1\left(\frac{(\rho c_p)_{s_1}}{(\rho c_p)_f}\right)\right]+\varphi_2(\rho c_p)_{s_2}$

The attached boundary conditions are:

$$\begin{aligned} &u = 0, \quad v = v_w, \quad T = T_w = ax^{\lambda} + T_\infty, \quad \text{on} \quad y = 0, \quad x \geqslant 0, \\ &u = 0, \quad T \to T_\infty \quad \text{as} \quad y \to \infty. \end{aligned} \tag{4}$$

where u and v are components of velocity along x and y directions, with thin boundaries $r = x\sin\omega$. The density of the HNF is ρ_{hnf}. The dynamic viscosity of HNF is μ_{hnf}. T is the temperature of HNF and q_r is a flux which depends on the temperature of the body. g is a gravitational acceleration and v_w is a suction velocity on the surface of inverted cone. According to the Rosseland approximation[39,40] radiative heat flux is defined as:

$$q_r = -\frac{4\sigma^{**}}{3k^{**}}\frac{\partial T^4}{\partial r}, \tag{5}$$

here σ^{**} and k^{**} are the Stefan–Boltzmann constant and coefficient of mean proportion. Also we introduced the stream function Ψ as flows:

$$u = \frac{1}{r}\frac{\partial \Psi}{\partial y} \quad \text{and} \quad v = -\frac{1}{r}\frac{\partial \Psi}{\partial x}. \tag{6}$$

Now we introduce the following similarity transformations as:

$$\begin{aligned} &u = \frac{v_f}{x}f' Gr_x^{\frac{1}{4}}, \quad \eta = \frac{x}{y}Gr_x^{\frac{1}{4}}, \quad \theta(\eta) = \frac{T_\infty - T}{T_\infty - T}, \\ &v = \frac{v_f}{x}Gr_x^{\frac{1}{4}}\left(f - \eta f'\right), \Psi = v_f r Gr_x^{\frac{1}{4}} f(\eta), \end{aligned} \tag{7}$$

where Gr_x is Rayleigh number and mathematically given by:

$$Gr_x = \frac{g(\rho\beta)_{hnf}\cos\omega\,(T_w - T_\infty)x^3}{v_f^2}. \tag{8}$$

Since Equation (1) is already satisfied and now we substitute the transformations defined in Equation (4) into the Equations (1) to (3) and we get following coupled ODEs:

$$\frac{1}{\Phi_1}f''' + \left(\frac{\lambda+7}{4}\right)ff'' - \left(\frac{\lambda+1}{4}\right)(f')^2 - \frac{M^2 f'}{\Phi_2} + \theta = 0, \tag{9}$$

$$\frac{k_{hnf}}{\Phi_3 k_f}(1+N)\theta'' + P_r\left[\left(\frac{\lambda+7}{4}\right)f\theta' + Ec\left(f''\right)^2 - \lambda\theta f'\right] = 0. \tag{10}$$

$$\begin{aligned} &f - S = 0, \quad f' = 0, \quad \theta - 1 = 0, \quad \text{as} \quad \eta = 0, \\ &f' = 0, \quad \theta = 0, \quad \text{as} \quad \eta = \infty. \end{aligned} \tag{11}$$

The mathematical expressions of Φ_1, Φ_2, and Φ_3 are defined as:

$$\Phi_1 = (1-\varphi_2)^{2.5}(1-\varphi_1)^{2.5}\left[(1-\varphi_2)\left\{(1-\varphi_1)+\varphi_1\left(\frac{\rho_{s_1}}{\rho_f}\right)\right\}\right]+\varphi_2\left(\frac{\rho_{s_2}}{\rho_f}\right), \tag{12}$$

$$\Phi_2 = (1-\varphi_2)\left[(1-\varphi_1)+\varphi_1\left(\frac{\rho_{s_1}}{\rho_f}\right)\right]+\varphi_2\left(\frac{\rho_{s_2}}{\rho_f}\right), \tag{13}$$

$$\Phi_3 = (1-\varphi_2)\left[(1-\varphi_1)+\varphi_1\frac{\left(\rho c_p\right)_{s_1}}{\left(\rho c_p\right)_f}\right]+\varphi_2\frac{\left(\rho c_p\right)_{s_2}}{\left(\rho c_p\right)_f}. \tag{14}$$

The mathematical expression of prominence fluidic parameter of interest for proposed nanofluidic system are defined as:

$$M = \frac{\sigma_{hnf}B_0^2x^2}{\mu_f Gr_x^{\frac{1}{2}}}, \quad S = \frac{v_w x}{v_f Gr_x^{\frac{1}{2}}}, \quad Ec = \frac{\mu_f x^2}{Gr_x^{\frac{1}{2}}},$$
$$N = \frac{16T_\infty^3x^2}{3k^{**}k\mu_f\left(c_p\right)_f Gr_x^{\frac{1}{2}}}, \quad Pr = \frac{\mu_f\left(c_p\right)_f}{k_f}. \tag{15}$$

where, Pr represents Prandtl number, Ec is Eckert number, M is Hartman number, and N is radiation parameter respectively. Here $f(\eta) = S$ when $\eta = 0$ with $S < 0$ being suction case and $S > 0$ shows injection case. The Nusselt number Nu and skin friction coefficient C_f are defined as:

$$Nu = \frac{q_w}{k_{hnf}\left(T_w - T_\infty\right)}, \quad C_f = \frac{\tau_w}{\rho_{hnf}u_w^2}. \tag{16}$$

The expression of shear stress on the surface of the cone is indicated by τ_w and given as:

$$\tau_w = \mu_{hnf}\left(\frac{\partial u}{\partial y}\right), \quad \text{at} \quad y = 0. \tag{17}$$

The q_w shows the heat flux from the surface of the cone and defined as:

$$q_w = (q_r)_w - k_{hnf}\left(\frac{\partial T}{\partial y}\right), \quad \text{at} \quad y = 0. \tag{18}$$

After solving from Equations (16) to (18), we obtain the dimensionless form of Nusselt number Nu_x and skin-friction $C_f Gr_x^{\frac{1}{4}}$ which are given as:

$$C_f Gr_x^{\frac{1}{4}} = \frac{f''(0)}{(1-\varphi)^{2.5}}, \quad Nu_x = -\left(N + \frac{k_{hnf}}{k_f}\right)\theta'(0). \tag{19}$$

3 | RESULTS AND DISCUSSION

Here, the empirical results of fluidic parameters on fluid velocity and temperature distributions are analyzed graphically. Furthermore, tabular forms are created for relevant physical parameters namely, the Nusselt number and skin friction coefficient for various nano-materials shape factors throughout the conduct of HNF MoS_2-SiO_2/water and dotted lines will be used to show SiO_2/water NF results, respectively.

For this purpose, the coupled nonlinear ordinary differential system of the nanofluidic model is derived from governing PDEs by the exploitation of the non-dimensional similarity variables approach. The transformed nanofluidic differential system of ODEs presented in Equations (9) and (10) are tackled numerically along with attached boundary conditions Equation (12) by employing the Lobatto IIIA approach with MATLAB routine "bvp4c." Power law λ is

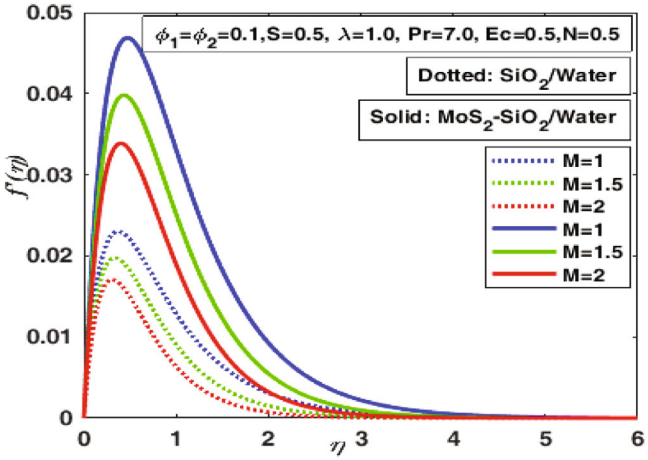

FIGURE 3 The influence of power law index on $f'(\eta)$.

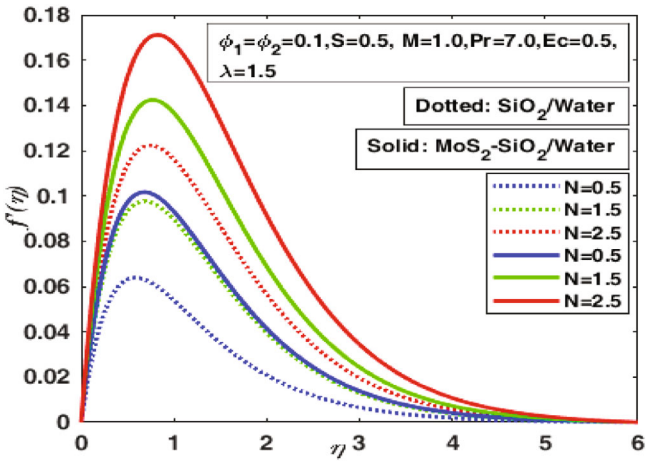

FIGURE 4 Influence of Hartmann number on $f'(\eta)$.

analyzed through Figure 3. The fluid is shown to decelerate with such addition in λ and this reduction in the fluid flow for NF compared to HNF is more pronounced.

Figure 4 shows the effect of a magnetic field parameter M on $f'(\eta)$, so it suffices that the existence of the magnetic field resists fluid flow for NF and HNF. Figure 5 is sketched to analyze the influence of N thermal radiation parameter on the velocity profile of NF and HNF, respectively. Here, N relates to the acceleration of flowing fluid and the density of the NF and HNFs at the boundary layer of momentum. Figure 6 shows the influence of parameter S on SiO_2/H_2O and MoS_2-SiO_2/H_2O NFs velocity. It is notable that S presents two cases, if $S > 0$, it presents the injection case and when $S < 0$, it presents the suction case. Moreover, the value of $f'(\eta)$, almost reaches 0.1 for $S = 0.2$ which is far greater than the value of $f'(\eta)$ for SiO_2/H_2O at the same value of S. This figure clearly shows that as S is increased, the velocity reduces as a result of the surface suction acting in opposition to the flow of fluid, which results in a reduction in velocity. Additionally, NF exhibits a far greater velocity decrease than HNF. It is notable that this difference is more significant as compared to other values of S. Furthermore, decreased NF velocity is significantly greater than the HNF. The influence of the volumetric fraction of both NFs is examined by Figure 7. It is shown that the velocity of fluid grows with the change in all volumetric fractions of NPs.

The SiO_2 volumetric-fraction of HNF has been settled at 1%. The increasing trend in fluid velocity is related to the point that HNF and NF dynamic viscosity is in inverse relation to volumetric fractions of nano-particles. As a result, the increase in ϕ_1 and ϕ_2 means a reduction in the base fluid viscosity and this accelerates the fluid flow. Furthermore, the fluid velocity is observed more in the case of the HNF. Eckert number Ec influences are indicated in Figure 8. It can be

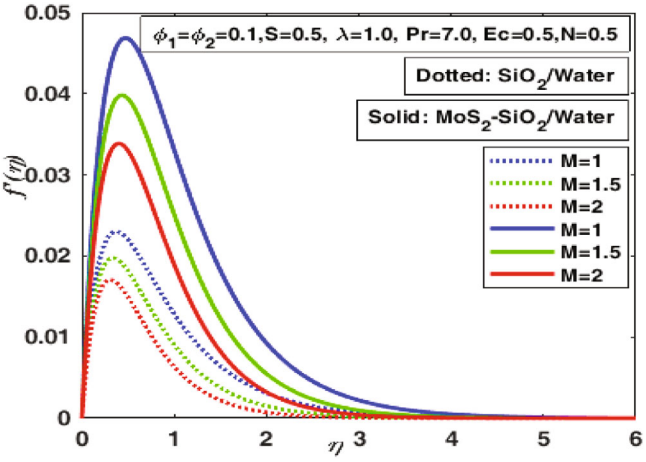

FIGURE 5 Effect of radiation parameter on $f'(\eta)$.

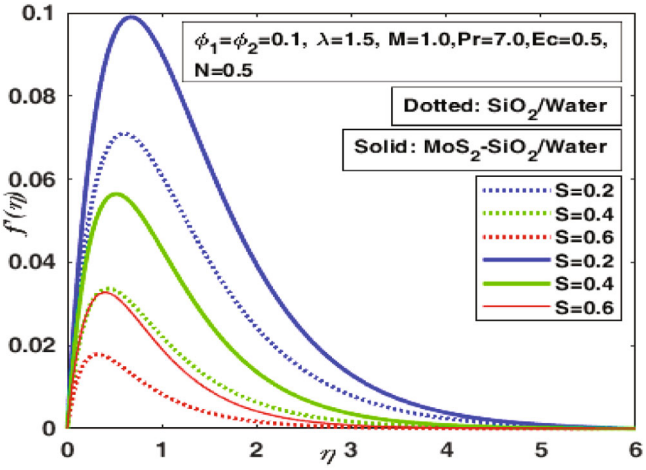

FIGURE 6 Effect of suction/injection parameter on $f'(\eta)$.

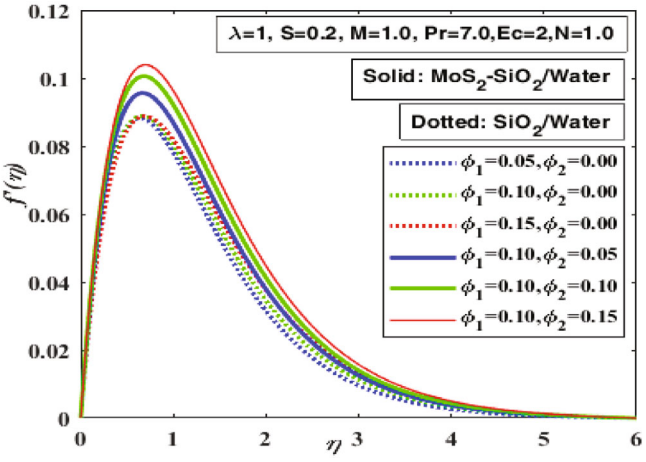

FIGURE 7 Impact of volumetric fractions ϕ_1 and ϕ_2 on $f'(\eta)$.

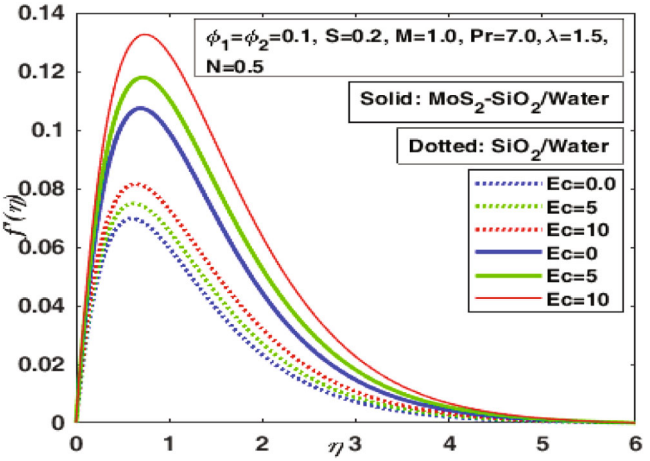

FIGURE 8 The effect of Eckert number on $f'(\eta)$.

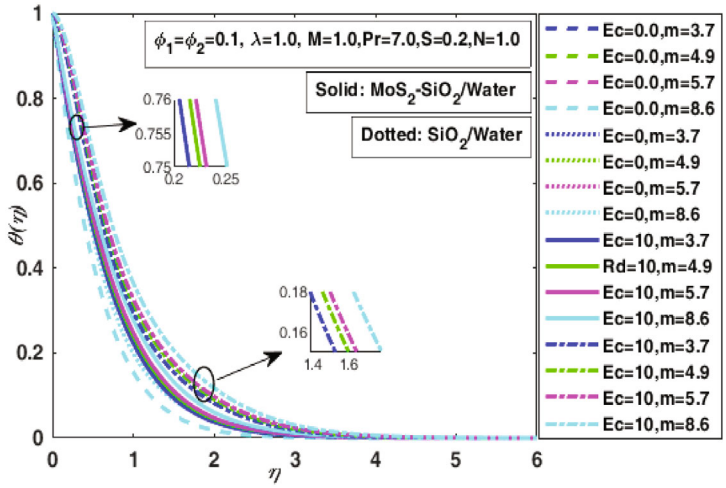

FIGURE 9 Impact of Eckert number on $\theta(\eta)$.

seen from this figure that the increased Eckert number leads to the acceleration of both forms of NF flow. Moreover, in the case of HNF, this change is considerably greater.

Figure 9 considering four different values of the nano-particles shaping factors for NF and also HNFS is arranged for various values of Eckert number. From such a figure it has been shown that the distribution of temperatures in both forms of NFs increases with the Eckert number. Figures 10 and 11 are plotted for increasing values of power law index λ and N (thermal radiation parameter) respectively.

From these graphical figures, it is also noted that the distributions of NF and HNF temperatures rise via an increase for both N and λ. The influence of volumetric fractions of the nano-particles is shown in Figure 12. It is noticed that throughout the presence of NF and HNF, the rise in volumetric fractions ϕ_1 and ϕ_2 contributes to increased temperature, respectively.

Table 4 reported the computed values of the Nusselt number in tabular form. The local Nusselt number upgraded by raising λ, Qh, We, Pr, and Bi while decay by increments in M^*, ϕ_w, δ, Sc, K_1, Nr, Nt, A^*, α, and β^*. The computed numerical data of Skin friction is rendered in Table 5. The skin friction grows for the magnetic parameter, Schmidt, and local Weisenberge number while declines for the temperature ratio parameter, unsteadiness, and shear rate parameter respectively.

The complexity of the proposed computational approach is interpreted in terms of tabulated data for each fluidic parameter. The mesh points analysis of the considered fluidic model acquired by the proposed numerical approach is

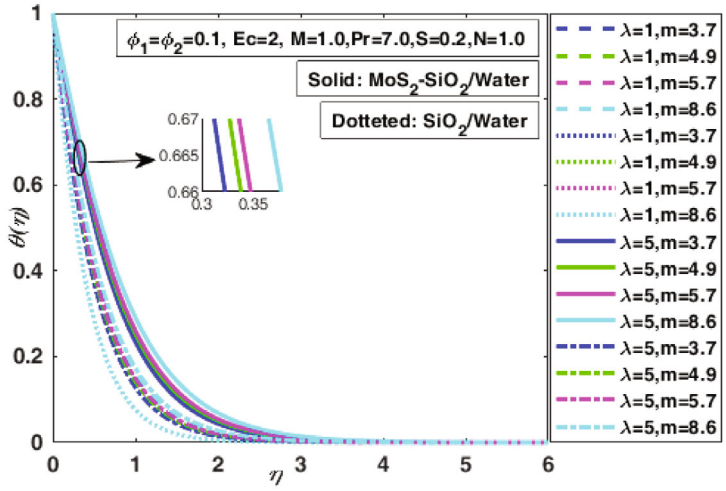

FIGURE 10 Impact of power law index on $\theta(\eta)$.

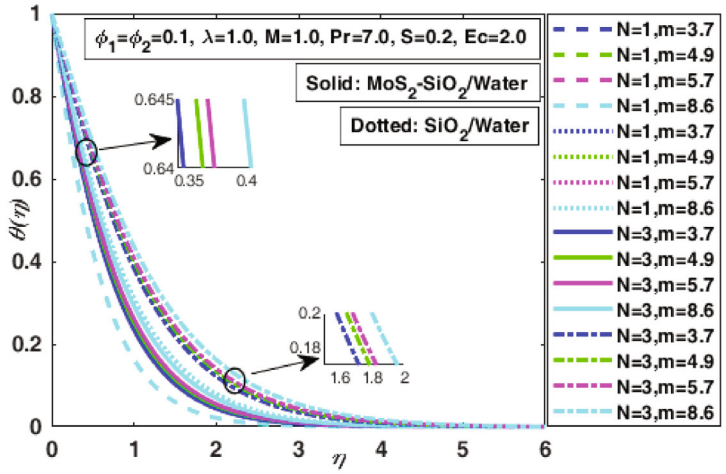

FIGURE 11 Impact of radiation parameter (N) and m on $\theta(\eta)$.

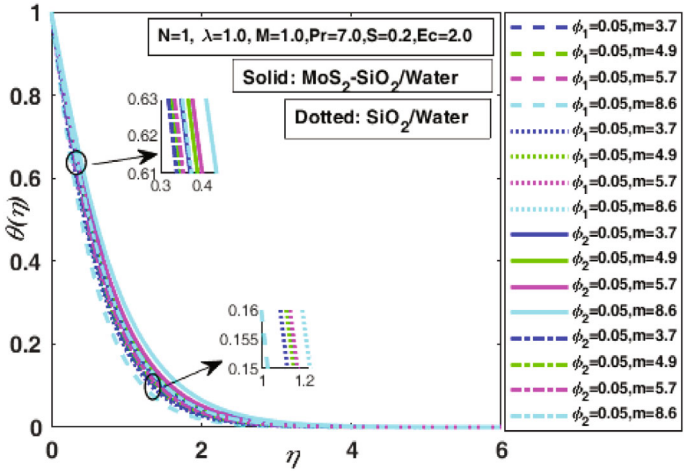

FIGURE 12 The impact of volumetric fractions ϕ_1 and ϕ_2 on $\theta(\eta)$.

TABLE 4 The numerical data analysis of local Nusselt number for SiO_2/H_2O and MoS_2-SiO_2/H_2O.

	SiO_2/H_2O			MoS_2-SiO_2/H_2O		
Parameter	$m = 3.7$	$m = 5.9$	$m = 7.9$	$m = 3.7$	$m = 5.9$	$m = 7.9$
ϕ_1/ϕ_2	3.6801	3.6062	3.5322	3.5336	3.4633	3.3963
λ	9.9452	10.6115	11.2739	6.4196	6.8556	7.2842
M	10.6115	10.6010	10.5918	6.8556	6.8331	6.8127
E	4.6754	4.0080	3.1504	3.4374	2.5739	1.3459
N	4.9096	3.2791	2.5856	3.4245	2.3957	1.9432
S	4.9258	8.6943	12.8249	3.6603	5.9823	8.6339

TABLE 5 The numerical data analysis of skin friction for SiO_2/H_2O and MoS_2-SiO_2/H_2O.

	SiO_2/H_2O			MoS_2-SiO_2/H_2O		
Parameter	$m = 3.7$	$m = 5.9$	$m = 7.9$	$m = 3.7$	$m = 5.9$	$m = 7.9$
ϕ_1/ϕ_2	0.2131	0.2020	0.1920	0.3271	0.3112	0.2970
λ	0.4182	0.4062	0.3902	0.4314	0.4452	0.4488
M	0.2020	0.1876	0.1745	0.3112	0.2854	0.2616
E	0.3548	0.3708	0.3913	0.4634	0.4927	0.5337
N	0.3380	0.4303	0.4892	0.4500	0.5468	0.6078
S	0.4182	0.4182	0.4182	0.4182	0.4975	0.5067

TABLE 6 The effect of mesh points on convergence of SiO_2/H_2O and MoS_2-SiO_2/H_2O.

		SiO_2/H_2O			MoS_2-SiO_2/H_2O		
Convergence limit	**Scenarios**	**Case-1**	**Case-2**	**Case-3**	**Case-1**	**Case-2**	**Case-3**
1E-09	1	1342	1425	1589	1527	1539	1668
	2	1699	1789	1789	1790	1199	1199
	3	1425	1271	1395	1539	1474	1673
	4	1373	1727	1530	1179	1565	1254
	5	1392	1673	1536	1198	1559	1481
1E-12	1	1342	1425	1589	1527	1539	1668
	2	1699	1789	1789	1790	1199	1199
	3	1425	1271	1395	1539	1474	1673
	4	1373	1727	1530	1179	1565	1254
	5	1392	1673	1536	1198	1559	1481

tabulated in Table 6 while Table 7 depicted the computed values of residual error by Lobatto IIIA approach for each sundry physical fluidic parameter, enlisting five different scenarios and three cases for NF and HNF.

A comparative analysis is presented for the proposed method with other numerical methods. In Reference 41, the authors have presented the solution of the current problem by using the shooting method and Runge-Kutta method of order six and in Reference 40, the authors have presented the solutions by using the shooting algorithm. Here, the authors have compared the results for particular values of parameters of volumetric fractions and Nusselt numbers in Tables 8 and 9 for different values of λ. The current study has obtained better results as compared to Runge-Kutta and shooting methods and performed almost similar to both techniques while using a simplified and less complicated algorithm.

TABLE 7 The illustration of residual error analysis of SiO_2/H_2O and MoS_2-SiO_2/H_2O.

		SiO_2/H_2O			MoS_2-SiO_2/H_2O		
C L	Scenarios	Case-1	Case-2	Case-3	Case-1	Case-2	Case-3
	1	3.09E-11	2.68E-11	4.23E-11	1.93E-12	3.11E-12	4.57E-12
	2	2.20E-12	1.83E-12	1.47E-12	1.90E-12	7.57E-12	6.94E-12
1E-09	3	2.68E-11	7.88E-11	6.92E-10	3.11E-12	3.53E-12	3.99E-12
	4	6.99E-11	5.97E-12	9.89E-12	4.90E-11	3.00E-12	1.54E-11
	5	3.31E-12	1.54E-12	9.47E-13	7.47E-12	8.61E-13	6.24E-13
	1	3.09E-14	2.68E-14	4.23E-14	1.93E-15	3.11E-15	4.57E-15
	2	2.20E-15	1.83E-15	1.47E-15	1.90E-15	7.57E-15	6.94E-15
1E-12	3	2.68E-14	7.88E-14	6.92E-13	3.11E-15	3.53E-15	3.99E-15
	4	6.99E-14	5.97E-15	9.89E-15	4.90E-14	3.00E-15	1.54E-14
	5	3.31E-15	1.54E-15	9.47E-16	7.47E-15	8.61E-16	6.24E-16

TABLE 8 The comparison of C_f for volumetric fractions $\phi_1 = 0 = \phi_2$.

	Awad et al.[41]			
λ	BVP4c	RK6	Maraj et al.[40]	Our method
0	1.0857945	1.0857945	1.0857945	1.063245
0.3	1.0457628	1.0457628	1.0457628	1.057913
0.6	1.0122259	1.0122259	1.0122259	0.961136
1	0.9748621	0.9748621	0.9748621	0.983212

TABLE 9 The comparison of Nusselt no. for volumetric fractions $\phi_1 = 0 = \phi_2$, $N = 0$.

	Awad et al.[41]			
λ	BVP4c	RK6	Maraj et al.[40]	Our method
0	0.5063661	0.5063661	0.5063661	0.482139
0.3	0.5524177	0.5524177	0.5524177	0.579842
0.6	0.5915881	0.5915881	0.5915881	0.543161
1	0.6361635	0.6361635	0.6361635	0.613478

4 | CONCLUSION, NOVELTY, AND RECOMMENDATIONS

This article portrays a numerical investigation of porous surfaces for convection. The nanofluidic model is based on the inverted cone along with porous boundary for both NF SiO_2/water and HNF MoS_2-SiO_2/water respectively. We observed that fluid velocity reduces with a rise in λ and as compared to HNF. The decrease in the flow of fluid is greater in the case of NF. It is also observed that the flow of fluid for SiO_2/water NF decelerates more as compared to the HNF.

The fluid flow decelerates as λ increases, and NFs shows the deceleration more pronouncedly than HNFs. With a rise in $S > 0$, velocity decreases. Moreover, it has been observed that fluidic flow slows down more for SiO_2/water NF than for HNF. Both forms of NF flow are accelerated by a rise in Eckert number. In the case of HNF, this rise is also much greater. The momentum and fluid flow boundary layer thickness of NF and HNFs are accelerated by a rise in the heat radiation parameter N. For both NF and HNFs, the skin friction coefficient and Nusselt number rise as the volumetric fractions of nanoparticles increase by ϕ_1 and ϕ_2, respectively.

A HNF with blade-shaped nanoparticles also exhibits the highest skin friction coefficient and Nusselt number, whereas brick-shaped nanoparticles suspended in a NF exhibit the lowest. In the case of SiO_2/water NF, skin friction coefficient rises with an increase in suction parameter S, however the opposite trend is observed for MoS_2-SiO_2/water HNF. Brick shape nanoparticles hanged in SiO_2/water NF exhibit the lowest magnitude, and blade shape nanoparticles hanged in MoS_2-SiO_2/water HNF exhibit the highest magnitude. For both NF and HNFs, the Nusselt number rises with increasing the suction parameter values. As viscous dissipation and harmful radiation increase, skin friction coefficient rises and Nusselt's number falls. Exhaustive analysis of these statistics shows that the HNF plays a significant role in transport of fluids and an elevated temperature distribution for NF is achieved.

NOMENCLATURE

μ_{nf}, μ_{hnf}	Viscosity of NF and HNF
ρ_{nf}, ρ_{hnf}	Density of NF and HNF
$\frac{k_{nf}}{k_f}, \frac{k_{hnf}}{k_f}$	Thermal conductivity of NF and HNF
$(\rho c_p)_{nf}, (\rho c_p)_{hnf}$	Heat capacity of NF and HNF
v_w	Suction velocity
q_r	Radiative heat flux
σ^{**}	Stefan Boltzmann constant
k^{**}	Coefficient of mean proportion
ψ	Stream function
Gr_x	Rayleigh number
Pr	Prandtl number
Ec	Eckert number
M	Hartmann number
N	Radiation parameter
Nu	Nusselt number
$S<0$	Suction case
$S>0$	Injection case
C_f	Skin friction coefficient
τ_w	Shear stress
Nu_x	Local Nusselt number
λ	Power law index
T_w	Wall temperature of inverted cone

AUTHOR CONTRIBUTIONS

Syed Ibrar Hussain: investigation (equal); methodology (equal); validation (equal); writing – original draft (equal). **Iftikhar Ahmad:** project administration (equal); supervision (equal). **Muhammad Asif Zahoor Raja:** formal analysis (equal); resources (equal). **Ch Muhammad Zulfiqar Umer:** investigation (equal); methodology (equal); validation (equal); writing – review and editing (equal).

CONFLICT OF INTEREST STATEMENT

There are no significant financial or non-financial objectives of the authors to disclose.

PEER REVIEW

The peer review history for this article is available at https://publons.com/publon/10.1002/eng2.12660.

DATA AVAILABILITY STATEMENT

The datasets created for and/or used in the analysis of the current research are accessible upon request.

ORCID

Syed Ibrar Hussain https://orcid.org/0000-0002-9391-3858

REFERENCES

1. Ratha P, Mishra S, Tripathy R. Exploration of dissipative heat energy in conjunction with various thermophysical properties of nanofluids: water and ethylene glycol base fluids. *Int Commun Heat Mass Transf*. 2022;138:106423.
2. Smaisim GF, Mohammed DB, Abdulhadi AM, et al. Nanofluids: properties and applications. *J Solgel Sci Technol*. 2022;104(1):1-35.
3. Yasmin H, Giwa SO, Noor S, Sharifpur M. Thermal conductivity enhancement of metal oxide nanofluids: a critical review. *Nanomaterials*. 2023;13(3):597.
4. Shoaib M, Tabassum R, Nisar KS, et al. A design of neuro-computational approach for double-diffusive natural convection nanofluid flow. *Heliyon*. 2023;9:e14303.
5. Younes H, Mao M, Murshed SS, Lou D, Hong H, Peterson G. Nanofluids: key parameters to enhance thermal conductivity and its applications. *Appl Therm Eng*. 2022;207:118202.
6. Khan Z, Zuhra S, Islam S, Raja MAZ, Ali A. Modeling and simulation of Maxwell nanofluid flows in the presence of Lorentz and Darcy–Forchheimer forces: toward a new approach on Buongiornos model using artificial neural network (ANN). *Eur Phys J Plus*. 2023;138(1):107.
7. Endalew MF, Sarkar S. Numerical exploration of forced convection hydromagnetic hyperbolic tangent nanofluid flow over a permeable wedge with melting heat transfer. *Sci Rep*. 2023;13(1):3515.
8. Oke AS. Heat and mass transfer in 3D MHD flow of EG-based ternary hybrid nanofluid over a rotating surface. *Arab J Sci Eng*. 2022;47:16015-16031.
9. Bhatti M, Ellahi R, Doranehgard MH. Numerical study on the hybrid nanofluid (Co_3O_4-Go/H_2O) flow over a circular elastic surface with non-Darcy medium: application in solar energy. *J Mol Liq*. 2022;361:119655.
10. Zainodin S, Jamaludin A, Nazar R, Pop I. Effects of higher order chemical reaction and slip conditions on mixed convection hybrid ferrofluid flow in a Darcy porous medium. *Alex Eng J*. 2023;68:111-126.
11. Shoaib M, Raja MAZ, Sabir MT, et al. Numerical analysis of 3-D MHD hybrid nanofluid over a rotational disk in presence of thermal radiation with joule heating and viscous dissipation effects using Lobatto IIIA technique. *Alex Eng J*. 2021;60(4):3605-3619.
12. Ali S, Raja MAZ, Cheema TN, Ahmad I, Mian N, Shoaib M. Analysis of Williamson nanofluid with velocity and thermal slips past over a stretching sheet by Lobatto IIIA numerically. *Therm Sci*. 2021;25:2795-2805.
13. Choi S, Singer D, Wang H, et al. Developments and applications of non-Newtonian flows. *ASME Fed*. 1995;66:99-105.
14. Khan W, Pop I. Boundary-layer flow of a nanofluid past a stretching sheet. *Int J Heat Mass Transf*. 2010;53(11-12):2477-2483.
15. Ramzan M, Dawar A, Saeed A, Kumam P, Watthayu W. MHD flow of micropolar and Williamson fluids over a bi-directional stretching sheet. *Eur Phys J Plus*. 2022;137(7):869.
16. Na T-Y, Chiou J. Laminar natural convection over a frustum of a cone. *Appl Sci Res*. 1979;35(5-6):409-421.
17. Yih K. Coupled heat and mass transfer by free convection over a truncated cone in porous media: VWT/VWC or VHF/VMF. *Acta Mech*. 1999;137(1-2):83-97.
18. El-Aziz MA. Effect of time-dependent chemical reaction on stagnation point flow and heat transfer over a stretching sheet in a nanofluid. *Phys Scr*. 2014;89(8):085205.
19. Ahmad I, Hussain SI, Usman M, Ilyas H. On the solution of Zabolotskaya–Khokhlov and diffusion of oxygen equations using a Sinc collocation method. *Partial Differ Equ Appl Math*. 2021;4:100066.
20. Ahmad I, Hussain SI, Ilyas H. Numerical solutions of Schrödinger wave equation and transport equation through Sinc collocation method. *Nonlinear Dyn*. 2021;105(1):691-705.
21. Ahmad I, Ahmad S, Kutlu K, Ilyas H, Hussain SI, Rasool F. On the dynamical behavior of nonlinear Fitzhugh–Nagumo and Bateman–Burger equations in quantum model using Sinc collocation scheme. *Eur Phys J Plus*. 2021;136(11):1-24.
22. Ahmad I, Ilyas H, Kutlu K, Anam V, Hussain SI, Guirao JLG. Numerical computing approach for solving Hunter-Saxton equation arising in liquid crystal model through Sinc collocation method. *Heliyon*. 2021;7(7):e07600.
23. Ahmad I, Hussain SI, Raja MAZ, Shoaib M. Transportation of hybrid MoS 2–SiO 2/EG nanofluidic system toward radially stretched surface. *Arab J Sci Eng*. 2022;48:953-966.
24. Noghrehabadi A, Behseresht A, Ghalambaz M. Natural convection of nanofluid over vertical plate embedded in porous medium: prescribed surface heat flux. *Appl Math Mech*. 2013;34(6):669-686.
25. Zeeshan A, Ellahi R, Hassan M. Magnetohydrodynamic flow of water/ethylene glycol based nanofluids with natural convection through a porous medium. *Eur Phys J Plus*. 2014;129(12):261.
26. Ellahi R, Hassan M, Zeeshan A. Shape effects of nanosize particles in Cu–H_2O nanofluid on entropy generation. *Int J Heat Mass Transf*. 2015;81:449-456.
27. Namburu PK, Kulkarni DP, Misra D, Das DK. Viscosity of copper oxide nanoparticles dispersed in ethylene glycol and water mixture. *Exp Therm Fluid Sci*. 2007;32(2):397-402.
28. Chen H, Ding Y, Tan C. Rheological behaviour of nanofluids. *New J Phys*. 2007;9(10):367.
29. Chen H, Ding Y, Lapkin A. Rheological behaviour of nanofluids containing tube/rod-like nanoparticles. *Powder Technol*. 2009;194((1-2)):132-141.
30. Masoumi N, Sohrabi N, Behzadmehr A. A new model for calculating the effective viscosity of nanofluids. *J Phys D Appl Phys*. 2009;42(5):055501.
31. Afshari A, Akbari M, Toghraie D, Yazdi ME. Experimental investigation of rheological behavior of the hybrid nanofluid of MWCNT–alumina/water (80%)–ethylene-glycol (20%). *J Therm Anal Calorim*. 2018;132(2):1001-1015.

32. Kang HU, Kim SH, Oh JM. Estimation of thermal conductivity of nanofluid using experimental effective particle volume. *Exp Heat Transf*. 2006;19(3):181-191.
33. Nagoor AH, Alaidarous ES, Sabir MT, Shoaib M, Raja MAZ. Numerical treatment for three-dimensional rotating flow of carbon nanotubes with Darcy–Forchheimer medium by the Lobatto IIIA technique. *AIP Adv*. 2020;10(2):025016.
34. Uddin I, Akhtar R, Zhiyu Z, Islam S, Shoaib M, Raja MAZ. Numerical treatment for Darcy-Forchheimer flow of Sisko nanomaterial with nonlinear thermal radiation by Lobatto IIIA technique. *Math Probl Eng*. 2019;2019:8974572.
35. Uddin I, Akhtar R, Khan MAR, et al. Numerical treatment for fluidic system of activation energy with non-linear mixed convective and radiative flow of magneto nanomaterials with Naviers velocity slip. *AIP Adv*. 2019;9(5):055210.
36. Ouyang C, Akhtar R, Raja MAZ, Touseef Sabir M, Awais M, Shoaib M. Numerical treatment with Lobatto IIIA technique for radiative flow of MHD hybrid nanofluid (Al_2O_3Cu/H_2O) over a convectively heated stretchable rotating disk with velocity slip effects. *AIP Adv*. 2020;10(5):055122.
37. Sun T-C, Uddin I, Raja MAZ, et al. Numerical investigation of thin-film flow over a rotating disk subject to the heat source and nonlinear radiation: Lobatto IIIA approach. *Waves Random Complex Media*. 2022;32:1-166.
38. Faisal M, Mabood F, Badruddin I. On numerical analysis of hydromagnetic radiative Jeffery nanofluid flow by variable thickness surface with activation energy and unsteadiness aspects. *Waves Random Complex Media*. 2022;32(5):554-573.
39. Ghoneim ME, Khan Z, Zuhra S, Ali A, Tag-Eldin E. Numerical solution of Rosselands radiative and magnetic field effects for Cu-kerosene and Cu-water nanofluids of Darcy-Forchheimer flow through squeezing motion. *Alex Eng J*. 2023;64:191-204.
40. Maraj E, Iqbal Z, Azhar E, Mehmood Z. A comprehensive shape factor analysis using transportation of MoS_2-SiO_2/H_2O inside an isothermal semi vertical inverted cone with porous boundary. *Results Phys*. 2018;8:633-641.
41. Awad F, Sibanda P, Motsa SS, Makinde OD. Convection from an inverted cone in a porous medium with cross-diffusion effects. *Comput Math Appl*. 2011;61(5):1431-1441.

How to cite this article: Hussain SI, Ahmad I, Raja MAZ, Umer CMZ. A computational convection analysis of SiO_2/water and MoS_2-SiO_2/water based fluidic system in inverted cone. *Engineering Reports*. 2023;5(11):e12660. doi: 10.1002/eng2.12660